Author Manuscript

Author Manuscript

Author Manuscript

Author Manuscript

HHS Public Access

Author manuscript

Plant J. Author manuscript; available in PMC 2019 January 01.

Published in final edited form as:

Plant J. 2018 January ; 93(1): 50–65. doi:10.1111/tpj.13756.

Identification and functional characterization of diterpene synthases for triptolide biosynthesis from *Tripterygium wilfordii*

Ping Su[1,2], **Hongyu Guan**[1,2], **Yujun Zhao**[1], **Yuru Tong**[1,2,6], **Meimei Xu**[5], **Yifeng Zhang**[1,2], **Tianyuan Hu**[2], **Jian Yang**[1], **Qiqing Cheng**[1,2,4], **Linhui Gao**[1,2], **Yujia Liu**[2], **Jiawei Zhou**[2], **Reuben J. Peters**[5], **Luqi Huang**[1,*], and **Wei Gao**[2,3,*]

[1]State Key Laboratory Breeding Base of Dao-di Herbs, National Resource Center for Chinese Materia Medica, China Academy of Chinese Medical Sciences, Beijing, China

[2]School of Traditional Chinese Medicine, Capital Medical University, Beijing, China

[3]Beijing Key Lab of TCM Collateral Disease Theory Research, Capital Medical University, Beijing, China

[4]State Key Laboratory of Quality Research in Chinese Medicine, Macau University of Science and Technology, Avenida Wai Long, Taipa, Macau, China

[5]Roy J. Carver Department of Biochemistry, Biophysics & Molecular Biology, Iowa State University, Ames, IA, USA

[6]School of Traditional Chinese Materia Medica, Shenyang Pharmaceutical University, Shenyang, China

SUMMARY

Tripterygium wilfordii has long been used as a medicinal plant, and exhibits impressive and effective anti-inflammatory, immunosuppressive and anti-tumor activities. The main active ingredients are diterpenoids and triterpenoids, such as triptolide and celastrol, respectively. A major challenge to harnessing these natural products is that they are found in very low amounts *in planta*. Access has been further limited by the lack of knowledge regarding the underlying biosynthetic pathways, particularly for the *abeo*-abietane tri-epoxide lactone triptolide. Here suspension cell cultures of *T. wilfordii* were found to produce triptolide in an inducible fashion, with feeding studies indicating that miltiradiene is the relevant abietane olefin precursor. Subsequently, transcriptome data was used to identify eight putative (di)terpene synthases that were then characterized for their potential involvement in triptolide biosynthesis. This included not only biochemical studies that revealed the expected presence of class II diterpene cyclases that produce the intermediate copalyl diphosphate (CPP), along with the more surprising finding of an

*For correspondence: Luqi Huang (huangluqi01@126.com), Wei Gao (weigao@ccmu.edu.cn).

Accession Numbers

The Illumina-derived nucleotide sequences reported in this paper have been submitted to the short-read archive (SRA) at NCBI with the following accession numbers: SRR6001265. Sequence data from this article can be found in the GenBank/EMBL data libraries with the following accession numbers: TwTPS7v2 (AKM28412); TwCPS2 (AKM28413); TwTPS3v2 (AKM28414); TwTPS9v2 (KX931054); TwTPS27v2 (ARQ20737); TwKSL1 (KX931055); TwTPS16v2 (AKM28415).

CONFLICT OF INTEREST STATEMENT

The authors declare that they have no conflict of interest in accordance with the journal policy.

Author Manuscript Author Manuscript Author Manuscript Author Manuscript

atypical class I (di)terpene synthase that acts on CPP to produce the abietane olefin miltiradiene, but also their sub-cellular localization and, critically, genetic analysis. In particular, RNA interference targeting either both of the CPP synthases, *TwTPS7v2* & *TwTPS9v2*, or the subsequently acting miltiradiene synthase, *TwTPS27v2*, led to decreased production of triptolide. Importantly, these results then both confirm that miltiradiene is the relevant precursor and the relevance of the identified diterpene synthases, enabling future studies of the biosynthesis of this important bioactive natural product.

Keywords

Tripterygium wilfordii; diterpene synthase; RNA interference; miltiradiene; triptolide

INTRODUCTION

Tripterygium wilfordii Hook. f., commonly known as Lei Gong Teng in Chinese, has been used for centuries, mainly to treat rheumatoid arthritis (Tu, 2009). While the genus *Tripterygium* is known to produce many types of terpenoids, the major bioactive compounds in *T. wilfordii* seem to be diterpenoids, especially triptolide, a tri-epoxide lactone first identified by Kupchan *et al.* (1972), and related compounds. These natural products have aroused extensive interest due to their broad spectrum of anti-inflammatory, immunosuppressive, anti-cystogenesis, and anticancer activities (Tao and Lipsky, 2000; Gong *et al.,* 2008; Chen *et al.,* 2009; Leuenroth *et al.,* 2010; Titov *et al.,* 2011; Manzo *et al.,* 2012; Chugh *et al.,* 2012). In addition, triptolide exerts effects on central nervous system diseases, such as Parkinson's and Alzheimer's (Li *et al.,* 2003, 2004; Gao *et al.,* 2008; Nie *et al.,* 2012; Zheng *et al.,* 2013). However, these diterpenoids currently are exclusively derived from *Tripterygium* plants, with low yields, limiting our ability to investigate and apply these bioactive compounds. Elucidation of the biosynthetic pathways for these complex diterpenoids would enable increased access via metabolic engineering, either in the native plant or using a synthetic biology approach to introduce the pathway into a microbial host.

Triptolide is an abietane-type diterpenoid, which places it in the labdane-related super-family that is characterized by formation of the underlying hydrocarbon backbone from the general diterpenoid precursor (*E,E,E*)-geranylgeranyl diphosphate (GGPP) by a sequential pair of cyclization reactions (Peters, 2010). These are catalyzed firstly by class II diterpene cyclases, which contain a characteristic DxDD motif, and then subsequently acting class I diterpene synthases that contain a separate DDxxD motif instead (Peters, 2010). Despite their distinct catalytic activity, catalyzed in separate active sites defined by the noted motifs (Gao *et al.,* 2012), these enzymes are both members of the terpene synthase (TPS) family, with the class II diterpene cyclases making up the TPS-c sub-family and subsequently acting class I diterpene synthases comprising the TPS-e sub-family (Chen *et al.,* 2011).

More specifically, triptolide is presumably produced via initial cyclization of GGPP to copalyl diphosphate (CPP), with subsequent cyclization and rearrangement to an abietane-type diene olefin, which is then further transformed to triptolide. It has been suggested that this proceeds via the aromatized dehydroabietic acid, with subsequent 1,2-migration of the

Author Manuscript Author Manuscript Author Manuscript Author Manuscript

carboxylic acid (from carbon 4 → 3) to form the observed *abeo*-abietane backbone (Kutney & Han, 1996). Notably, the cyclohexa-1,4-diene arrangement of the abietane miltiradiene poises this for aromatization (Gao *et al.,* 2009), which readily occurs spontaneously (Zi & Peters, 2013). Thus, miltiradiene is a likely intermediate in triptolide biosynthesis (Figure 1).

Identification of the tissues where the compound of interest is produced and/or conditions that lead to increased accumulation can significantly aid elucidation of the underlying biosynthetic pathway. Consistent with previous results (Kutney *et al.,* 1980), we have recently developed suspension cell cultures of *T. wilfordii* that produce triptolide and related diterpenoids, as well as the triterpenoid celastrol (Su *et al.,* 2014). Here we report that feeding miltiradiene to these cultures increases triptolide production. In addition, we find that production of triptolide can be induced in these cultures, which were then subjected to RNA-Seq to generate a transcriptome. This dataset was mined to discover eight potential (di)terpene synthases, which were functionally characterized by sub-cellular localization and biochemical analysis, revealing two closely related CPP synthases (CPSs), TwTPS7v2 and TwTPS9v2, and a subsequently acting miltiradiene synthase, TwTPS27v2. Critically, RNA interference (RNAi) of *TwTPS7v2* and *TwTPS9v2*, or *TwTPS27v2*, reduced triptolide production, confirming not only the role of miltiradiene as a precursor, but also of these diterpene synthases in biosynthesis of this important diterpenoid natural product.

RESULTS

Suspension cell cultures can be used to illuminate triptolide biosynthetic pathway

As previously reported (Su *et al.,* 2014), we have established *T. wilfordii* suspension cell cultures. Critically, these were found to stably produce diterpenoids, particularly including triptolide, over a 3-year period. Briefly, these cultures were grown in defined medium in the dark at 25 °C on a rotary shaker and transferred to fresh medium every 18 d, with increases of 2.6-fold in the fresh weight of suspension cells over this time (Figure S1). These cultures were found to produce 53 ± 3 μg/g of triptolide in the suspension cells and 4.0 ± 0.2 mg/L in the medium (Figure 2C).

To compare the phytochemical complexity of these suspension cell cultures relative to whole plants, extracts from the cells and medium, as well as plant root, stem, leaf, and flower tissues, were analyzed by ultra-performance liquid chromatography-quadrupole time of flight-mass spectrometry (UPLC/Q-TOF MS). The plant samples, especially those from the roots traditionally associated with medicinal use, were largely composed of a variety of alkaloids (e.g. wilforgine and wilforine), with relatively small amounts of diterpenoids, including triptolide. By contrast, the suspension cell cultures appear to selectively accumulate diterpenoids and triterpenoids rather than alkaloids. Indeed, the suspension cultures accumulated triptolide at a higher level than the native plant, and this was particularly prevalent in the media, which exhibits a relatively simple phytochemical profile that presumably would assist purification of triptolide and/or related diterpenoids. Thus, these cultures represent a potential source of these natural products for commercial production. Perhaps more relevant here, these cultures further provide a system for investigation of the underlying biosynthetic network. For example, potential intermediates

Author Manuscript Author Manuscript Author Manuscript Author Manuscript

such as triptophenolide, triptinin B and triptoquinonide can be readily detected in the suspension cells (Table 1 and Figure 2).

Miltiradiene is a precursor to triptolide

Notably, miltiradiene, arguably the most likely olefin precursor to triptolide, was detectable in our suspension cell cultures (Figure S2). To further investigate the potential role of miltiradiene in triptolide biosynthesis, this abietane was fed to these cultures, which led to a statistically significant increase in triptolide accumulation relative to control cultures after 5 d (Figure 3). Altogether, this indicated that miltiradiene does serve as a precursor to triptolide, such that a class I diterpene synthase producing this olefin should be involved in the biosynthesis of these diterpenoids.

Triptolide production is induced by methyl jasmonate

Previous work has indicated that the production of (di)terpenoid natural products can be induced by the defense signalling molecule methyl jasmonate (MeJA), which is further useful for co-expression analysis. Indeed, the application of MeJA to *T. wilfordii* cell cultures led to increased production of triptolide, at least in the cells, as measured by UPLC analysis (Figure S3). Elevated levels of triptolide in MeJA-induced relative to control cultures were evident within 72 h, with even larger differences found in later time points – e.g., after 240 h triptolide levels were >3-fold higher, reaching just over 200 μg/g, in the induced suspension cells (Figure 4). While it seems worth mentioning that the ability to induce higher levels of triptolide may assist the potential use of these suspension cell cultures for larger-scale production of this and related diterpenoids, here this finding was used to assist elucidation of the underlying biosynthetic network.

Induced transcriptome of *T. wilfordii*

Based on the ability of MeJA to increase triptolide production, such induced suspension cells were subjected to deep transcriptome sequencing with the Illumina HiSeq 2000 platform. In total, 12.68 Gb of clean sequence was obtained after adapter related reads, low quality reads and reads containing unknown bases were removed from the raw reads (Table S1). A total of 90,801 transcripts were assembled with a mean length of 1,053 bp and an N50 of 1,837 bp (Table S2 and Figure S4).

Functional annotation was carried out using multiple databases, specifically Nr (NCBI non-redundant protein sequences), Nt (NCBI non-redundant nucleotide sequences), Pfam (Protein family), KOG/COG (Clusters of Orthologous Groups of proteins), Swiss-Prot (A manually annotated and reviewed protein sequence database), KO (KEGG Ortholog database) and GO (Gene Ontology). Relevant to triptolide biosynthesis, 27 unigenes potentially involved in such metabolism were found, including eight putative diterpene synthases, as defined by falling within either the TPS-c or TPS-e sub-families (Tables S3–4; Figure S5).

Cloning of putative diterpene synthases

To demonstrate the utility of the generated transcriptome for elucidation of triptolide biosynthesis, it was hypothesized that the diterpene synthases necessary for formation of

Author Manuscript Author Manuscript Author Manuscript Author Manuscript

miltiradiene should be present – i.e., among those in the transcriptome. Sequence analysis indicated that full-length open reading frames (ORFs) were not present for all eight putative diterpene synthases. Thus, full-length sequences were obtained by 5' and 3' rapid amplification of cDNA ends (RACE), also using RNA from induced suspension cells. This eventually led to cloning of cDNA for six distinct full-length diterpene synthases (Table S5).

The obtained putative diterpene synthases were subjected to phylogenetic analysis (Figures 5 and S6–7). During the course of our studies reports appeared describing similar, although not exactly identical genes (Anderson-Ranberg *et al.,* 2016; Hansen *et al.,* 2017a). These are presumably allelic to those identified here and, to be consistent with these recent reports, here we utilize nomenclature that reflects these presumed relationships. Four of those found here fall within the TPS-c sub-family and, hence, were expected to be class II diterpene cyclases. Three appeared to be allelic to previously identified genes and, accordingly, were named *TwTPS7v2, TwTPS3v2*, and *TwTPS9v2*, while the remaining gene was termed *TwCPS2*. However, in place of the highly conserved DxDD motif, TwCPS2 contains "$DTDC^{311}$", raising questions about its activity. The two remaining diterpene synthases fall within the TPS-e sub-family, which is anchored by the *ent*-kaurene synthases (KSs) required in vascular plants for gibberellin phytohormone metabolism, but also contains derived KS-like (KSL) enzymes (Zi *et al.,* 2014). One appeared to be allelic to a previously identified gene and, hence, was named *TwTPS16v2*, while the other appeared to be unique and was named *TwKSL1*.

Functional characterization of the putative class II diterpene cyclases

To determine the function of the putative class II diterpene cyclases, these were heterologously expressed in *E. coli*, and tested with GGPP as substrate via *in vitro* cell-free assays. For detection by gas chromatography-mass spectrometry (GC-MS), phosphatase was added to the assays upon completion to dephosphorylate both the substrate GGPP and any product, such as CPP, yielding geranylgeraniol (GGOH) and copalol, respectively. The production of CPP was detected for TwTPS7v2, TwTPS3v2 and TwTPS9v2 by comparison to the known activity of a CPS from *Salvia miltiorrhiza* (SmCPS1; Gao *et al.,* 2009) (Figure 6A), while no activity was detected for TwCPS2. Thus, *TwCPS2* appears to be an inactive pseudogene. Consistent with this hypothesis is both the phylogenetic distance of this from other (functional) members of the TPS-c sub-family, even within the *Tripterygium* genus (Figure 5), and the fact that the lack of activity goes beyond simple loss of the DxDD motif, as correcting this (i.e., by changing C311 to the Asp prototypically found at that position) did not restore any enzymatic activity to TwCPS2.

To determine the absolute stereochemistry of the CPP products of TwTPS7v2, TwTPS3v2 and TwTPS9v2, these were coupled to stereospecific class I diterpene synthases. In particular, the miltiradiene synthase from *S. miltiorhiza*, SmMS (Gao *et al.,* 2009), or KS from *Arabidopsis thaliana*, AtKS (Yamaguchi *et al.,* 1998), which are specific for CPP or *ent*-CPP, respectively (Gao *et al.,* 2009; Morrone *et al.,* 2009). *In vitro* cell-free assays were carried out in all six possible pairings, with the production of miltiradiene observed in assays with SmMS and either TwTPS7v2 or TwTPS9v2, while *ent*-kaurene was only observed in assays with AtKS and TwTPS3v2 (Figure 6B). Thus, consistent with recently reported work

Author Manuscript Author Manuscript Author Manuscript Author Manuscript

on their allelic variants (Anderson-Ranberg *et al.,* 2016; Hansen *et al.,* 2017a), both TwTPS7v2 and TwTPS9v2 produce CPP, while TwTPS3v2 produces *ent*-CPP.

Functional characterization of putative class I diterpene synthases

To determine the function of the two putative class I diterpene synthases, they were recombinantly expressed in *E. coli* and subjected to *in vitro* cell-free assays in combination with either TwTPS7v2 or TwTPS3v2 (providing CPP or *ent*-CPP, respectively). Neither TwKSL1 or TwTPS16v2 produced miltiradiene. Instead, both were only active with *ent*-CPP. Consistent with the very recently reported activity of its allelic variant (Hansen *et al.,* 2017a), TwTPS16v2 produced largely 16α-hydroxy-*ent*-kaurane, along with small amounts of *ent*-kaurene (Figure S8), which was further confirmed by co-expressing this with TwTPS3v2 in yeast (*Saccharomyces cerevisiae*). TwKSL1 was found to produce a mixture of diterpenes, the major components of which were identified upon incorporation into a modular metabolic engineering system in *E. coli* (Cyr *et al.,* 2007), and comparison to already characterized enzymes (Jia & Peters, 2016), as *ent*-pimara-8(14),15-diene and small amounts of 8α-hydroxy-*ent*-pimar-15-ene, as well as minor amounts of *ent*-kaurene (Figure 6C).

Interestingly, the production of 16α-hydroxy-*ent*-kaurane has been previously shown to critically depend on the identity of a specific residue, which is conserved as methionine in KSs, but is a smaller residue in diterpene synthases that produce 16α-hydroxy-*ent*-kaurane instead, with corresponding site-directed mutagenesis of this residue leading to substantial changes in product outcome (Kawaide *et al.,* 2011; Zerbe *et al.,* 2012; Irmisch *et al.,* 2015). TwTPS16v2 contains an alanine at this position and, consistent with previous reports, substitution of Met leads to predominant production of *ent*-kaurene, with smaller amounts of 16α-hydroxy-*ent*-kaurane, from *ent*-CPP by the resulting mutant TwTPS16v2:A608M (Figure S8). The result, together with a report identifying two key residues of TwTPS14 and TwTPS21 by Hansen *et al.* (2017b), highlights the evolutionary potential of this enzymatic family to drive rapid diversification of plant diterpene biosynthesis through neo-functionalization (Hansen *et al.,* 2017b).

Identification of a miltiradiene synthase

Given the data indicating a role for miltiradiene in triptolide biosynthesis, it was hypothesized that an alternative terpene synthase responsible for its formation must be expressed in the *T. wilfordii* suspension cell cultures. Hence, we screened the transcriptome dataset using the amino acid sequence of the known miltiradiene synthase from *Salvia miltiorrhiza* (SmMS; Gao *et al.*, 2009), as the probe sequence (with a cutoff E-value of $< e^{-10}$). In total, 6 potential terpene synthases were found, including two of the already characterized diterpene synthases, two that fall within the TPS-a sub-family and appear to be sesquiterpene synthases, and two that fall within the TPS-b sub-family, which usually indicates that these would be monoterpene synthases (Table S6). However, consistent with a very recent report that appeared during the course of our studies (Hansen *et al.*, 2017a), we also found that one of these, upon recombinant expression in *E. coli* and subsequent *in vitro* cell-free assays in combination with TwTPS7v2, produces miltiradiene (Figure 6D). Given

Author Manuscript Author Manuscript Author Manuscript Author Manuscript

that this TPS appears to be allelic to the previously identified miltiradiene synthase, sharing 98.0% identity, to be consistent with that previous report, this is named here TwTPS27v2.

Use of TwTPS7v2/TwTPS9v2 and TwTPS27v2 in metabolic engineering

Yeast has been engineered to produce miltiradiene using the relevant diterpene synthases from *S. miltiorrhiza* (SmCPS1 and SmMS), including the use of gene fusions between *SmCPS1* and *SmMS*, which led to increased yield when expressed in the order SmMS-SmCPS1 (Zhou *et al.,* 2012). Here the utility of the relevant diterpene synthases from *T. wilfordii* for similar engineering was investigated. However, the yield from co-expression of TwTPS27v2 with either TwTPS7v2 or TwTPS9v2 in appropriately engineered yeast, which was equivalent to each other (Figure S9A), was not found to be significantly better than that previously reported using SmCPS1 and SmMS (Zhou *et al.,* 2012). Moreover, fusing TwTPS7v2 and TwTPS27v2, in either orientation, actually significantly decreased the yield of miltiradiene, to less than 5% of the strain separately expressing each of these enzymes (Figure S9B). Indeed, unlike SmCPS1 and SmMS (Zhou *et al.,* 2012), TwTPS7v2 and TwTPS27v2 do not seem to interact, consistent with negative results from yeast two-hybrid assays with these (Figure S10).

Subcellular localization

Particularly given that diterpene biosynthesis is initiated in plastids, separate from the cytosolic location presumed for monoterpene synthases (Chen *et al.,* 2011), to verify the role of TwTPS27v2 and the other diterpene synthases, it seemed worth investigating their sub-cellular localization. Accordingly, recombinant plasmids containing the ORFs of these genes fused with that for a green fluorescent protein (GFP) were transformed into *N. benthamiana* leaves, which were then examined for GFP localization (Figure 7). All GFP signals for TwTPS7v2, TwTPS3v2, TwTPS9v2 and TwTPS27v2 were mainly found in chloroplasts, while those for TwKSL1 and TwTPS16v2 were found both in chloroplast and cytoplasm, supporting roles for all of these in diterpene biosynthesis. However, consistent with the hypothesis that *TwCPS2* is a non-functional pseudo-gene, the GFP signal for TwCPS2 produced a typical cytoplasm localization pattern.

Induction of diterpene synthase transcription

To further investigate the potential role of the functionally characterized diterpene synthases in triptolide biosynthesis, their transcriptional response to MeJA was investigated. Transcript levels were measured by qRT-PCR in suspension cells after induction with MeJA. This revealed increased mRNA levels, peaking at 12 or 24 h, for all the diterpene synthases investigated here, except TwKSL1 (Figure 8).

RNAi of both TwTPS7v2 and TwTPS9v2, or TwTPS27v2

To provide more direct evidence of a role in triptolide biosynthesis for TwTPS7v2 and/or TwTPS9v2, as well as TwMS and, hence, miltiradiene, RNAi was employed with suspension cell cultures. Given the high identity between TwTPS7v2 and TwTPS9v2 (98.5%), both were targeted together using a stretch of identical sequence in the RNAi construct. While this only led to reductions of just over 30% in the transcript level of both *TwTPS7v2* and

Author Manuscript Author Manuscript Author Manuscript Author Manuscript

TwTPS9v2, transcript levels for *TwCPS2* and *TwTPS3v2* were not affected, and triptolide accumulation was nevertheless decreased by almost 50% compared to control cultures transformed with the empty vector. When RNAi targeting *TwTPS27v2* was carried out, the transcript level of *TwTPS27v2* was similarly only reduced by ~30%, with no reduction in the levels of the related TPS-b sub-family members *TwTPS22v2, TwTPS23v2, TwTPS32*, and *TwTPS33*, triptolide accumulation was decreased by ~40% (Figure 9).

DISCUSSION

The ability of *T. wilfordii* suspension cell cultures to produce valuable terpenoids, particularly the *abeo*-abietane tri-expoxide triptolide, has long been appreciated (Kutney *et al.,* 1980). The suspension cell cultures used here constitutively produce 53 ± 3 μg/g of triptolide in the suspension cells and 4.0 ± 0.2 mg/L in the medium, which is slightly lower than that of recently reported *Tripterygium* adventitious root cultures (90 ± 80 μg/g in the adventitious roots and 4.7 ± 0.9 mg/L in the medium, Inabuy *et al.,* 2017). Here the utility of these cell cultures for investigation of triptolide biosynthesis was first demonstrated by not only finding that miltiradiene can be detected therein, but also that feeding this olefin leads to increased accumulation, as well as the presence of several other plausible biosynthetic intermediates. Notably, it was further shown that triptolide biosynthesis can be induced by MeJA in these cultures, which further increases their utility by providing a means for co-expression analysis.

To begin elucidating triptolide biosynthesis, an RNA-Seq approach was taken to generate an induced suspension cell culture transcriptome. The utility of this sequence data was demonstrated by identification of the diterpene synthases involved in production of miltiradiene and, hence, triptolide biosynthesis. These were found to consist of not only the expected class II diterpene cyclases that produce CPP, termed here TwTPS7v2 and TwTPS9v2, but also the unusual finding of a subsequently acting class I diterpene synthase, TwTPS27v2, which is not from the TPS-e sub-family that typically provides such enzymes in labdane-related diterpenoid biosynthesis (Zi *et al.,* 2014), rather being derived from the phylogenetically distinct TPS-b sub-family instead. While similar biochemical characterization has been very recently reported for both presumably allelic copies of these *T. wilfordii* diterpene synthases (Hansen *et al.,* 2017), as well as the orthologs from *T regelii* (Inabuy *et al.*, 2017), the data reported here go beyond this to unambiguously demonstrate the role of the characterized enzymes in triptolide biosynthesis. Most critically, in addition to showing sub-cellular localization of these enzymes to the plastid, where such diterpene biosynthesis occurs *in planta*, this includes genetic evidence, with RNAi knock-down of these genes leading to reduced triptolide levels. Thus, it is now clear that *TwTPS7v2, TwTPS9v2* and *TwTPS27v2* are involved in triptolide biosynthesis, and these then provide targets for *in planta* metabolic engineering efforts aimed at increasing yields of this valuable diterpenoid natural product. In addition, the unambiguous assignment of miltiradiene as the olefin precursor now enables further investigation of subsequently acting enzymes, such as cytochrome P450 mono-oxygenases, much as demonstrated in other (di)terpenoid biosynthetic networks (Kitaoka *et al.,* 2015), and enabled by the induced transcriptome reported here.

Author Manuscript Author Manuscript Author Manuscript Author Manuscript

EXPERIMENTAL PROCEDURES

Plant material, chemicals and reagents

The *T. wilfordii* suspension cells were cultured in Murashige & Skoog basal medium containing 0.5 mg/L 2,4-dichlorophenoxyacetic acid (2,4-D), 0.1 mg/L kinetin (KT), 0.5 mg/L indole-3-butytric acid (IBA), and 30 g/L sucrose (pH = 5.8) by incubation in the dark at 25 °C on a rotary shaker (Su *et al.,* 2014). After 10 days of cultivation, induced suspension cells were treated with methyl jasmonate (MeJA) in carrier solution (dimethyl sulfoxide) at the final concentration of 50 μM, while control cultures were only treated with same volume of carrier solution. *Nicotiana benthamiana* were grown in a greenhouse with a 16 h-light/8 h-dark cycle. Triptolide, wilforgine and wilforine were purchased from Chengdu Push Bio-Technology Co., Ltd (Chengdu, China). Celastrol, demethylzeylasteral and triptonide were purchased from Chengdu Must Bio-Technology Co., Ltd (Chengdu, China). Triptophenolide and neotriptophenolide were purchased from Shanghai yuanye Bio-Technology Co., Ltd (Shanghai, China). Dehydroabietic acid, triptinin B and triptoquinonide were purchased from BioBioPha Co., Ltd (Yunnan, China). All other reagents were purchased from Merck.

Metabolite analysis of suspension cell cultures and native plant

Solid samples were harvested and homogenized using Retsch MM400 mixer mill (Retsch GmbH, Haan, Germany), and placed in an ultralow-temperature refrigerator at 80 °C for at least 4 h prior to freeze drying for 48 h (EYELA FDU-1110, Tokyo, Japan). For each sample, aliquots of 50 mg were suspended in 1 mL of 80% (v/v) methanol overnight at room temperature, and then subjected to sonication in an ultrasonic water bath for 60 min. The supernatant was filtered through a 0.22-μm membrane filter (polytetrafluoroethylene) before further analysis. A medium aliquot of suspension cell cultures (generally 7.5 mL) was extracted twice with ethyl acetate (3 mL each time) by thorough mixing for 1 min at room temperature. The organic fractions were pooled and dried using a Nitrogen Evaporator (Baojingkeji, Henan, China). The residue was redissolved in 300 μL of 80% methanol and passed through a 0.22-μm membrane filter prior to injection into the UPLC/Q-TOF MS system for analysis.

The UPLC separation was performed using a Waters Acquity UPLC™ I-Class system (Waters Corp., Milford, MA, USA) with a Waters ACQUITY UPLC HSS T3 analytical column (2.1 mm × 100 mm, 1.8 μm) kept at 40 °C. The mobile phase, consisting of a mixture of 0.1% (v/v) acetic acid in water (A) and acetonitrile (B), was pumped at a flow rate of 0.5 mL/min. The gradient elution was programed as follows: 0 min at 30% B, 6 min at 45% B, 18 min at 60% B, 23 min at 90% B. The TOF MS experiments were performed using a Xevo G2-S QTOF MS system (Waters Corp., Milford, MA, USA). The experiment was performed in the ESI (+) ionization modes and the data acquisition modes were MS^E continuum. The source and desolvation temperature were 100 °C and 450 °C, respectively, and the desolvation gas flow rate was 900 L/h. The capillary voltage were 0.5 KV and the cone voltage was 40 V. The ramp collision energy was set as 20–40 eV for the high-energy scans. The data acquisition range was 50–1500 Da. The mass accuracy was maintained using a lock spray with leucine enkephalin (200 pg/μL, 10 μL/min) as the reference (*m/z*

Author Manuscript Author Manuscript Author Manuscript Author Manuscript

556.2771 ESI (+)). Data analysis was performed using the UNIFI Scientific Information System.

Feeding studies

Miltiradiene (13.6 mg) in 200 μL of methanol/DMSO (1/1, vol/vol) was fed to freshly sub-cultured suspension cells cultures (~1 g fresh weight suspension cells in 10 mL MS media in 50-mL flasks), and cells in control group were only treated with the same volume of carrier solution. After treatment, the cells were harvested in liquid nitrogen at 0, 1, 3 and 5 d, and the corresponding medium was stored at 4 °C. All the media (~ 10 mL) were extracted twice with ethyl acetate (5 mL each time) and the organic fractions were pooled dried in the 2.0-mL eppendorf tube as described above. Solid samples were homogenized and freeze dried, ~ 80 mg added to the 2.0-mL eppendorf tube, which were then extracted with 1.5 mL of 80% (v/v) as described above. The supernatant was filtered through a 0.22-μm membrane filter (polytetrafluoroethylene) for UPLC analysis. Additional details are provided in the supplemental METHODS.

RNA-Seq

Total RNA of the MeJA-induction 12–24–48 h suspension cells was isolated using the cetyltrimethylammonium bromide (CTAB) method (Del Sal *et al.,* 1989). The total RNA was treated with RNase-free DNase I (NEB, USA) and purified by RNA Purification Kit (Tiangen Biotech, Beijing, China). A total of 3 μg purified RNA was used as input material for the RNA sample preparations. Sequencing libraries were generated using NEBNext® Ultra™ RNA Library Prep Kit for Illumina® (NEB, USA) following the manufacturer's recommendations and index codes were added to attribute sequences to each sample. Briefly, mRNA was purified from total RNA using poly-T oligo-attached magnetic beads. Fragmentation was carried out using divalent cations under elevated temperature in NEBNext First Strand Synthesis Reaction Buffer (5×). First strand cDNA was synthesized using random hexamer primer and M-MuLV Reverse Transcriptase (RNase H^-). Second strand cDNA synthesis was subsequently performed using DNA Polymerase I and RNase H. Remaining overhangs were converted into blunt ends via exonuclease/polymerase activities. After adenylation of 3' ends of DNA fragments, NEBNext Adaptor with hairpin loop structure were ligated to prepare for hybridization. In order to preferentially select cDNA fragments of 150~200 bp length, the library fragments were purified with AMPure XP system (Beckman Coulter, Beverly, USA). Then 3 μl USER Enzyme (NEB, USA) was used with size-selected, adaptor-ligated cDNA at 37°C for 15 min followed by 5 min at 95 °C before PCR. Then PCR was performed with Phusion High-Fidelity DNA polymerase, Universal PCR primers and Index (X) Primer. Finally, PCR products were purified (AMPure XP system), and library quality assessed on the Agilent Bioanalyzer 2100 system.

The clustering of the index-coded samples was performed on a cBot Cluster Generation System using TruSeq PE Cluster Kit v3-cBot-HS (Illumina) according to the manufacturer's instructions. After cluster generation, the library preparations were sequenced on an Illumina Hiseq 2000 platform and paired-end reads were generated. Over 95% of these reads (63,401,185) were judged to be clean, and used for further analysis. The left files (read1 files) from all libraries/samples were pooled into one big left.fq file, and right files (read2

Author Manuscript Author Manuscript Author Manuscript Author Manuscript

files) into one big right.fq file. Transcriptome assembly was accomplished based on the left.fq and right.fq using Trinity (Grabherr *et al.*, 2011) with min_kmer_cov set to 2 by default and all other parameters also set to their default values. Gene function was annotated based on the following databases: Nr (NCBI non-redundant protein sequences), Nt (NCBI non-redundant nucleotide sequences), Pfam (Protein family), KOG/COG (Clusters of Orthologous Groups of proteins), Swiss-Prot (A manually annotated and reviewed protein sequence database), KO (KEGG Ortholog database), GO (Gene Ontology).

RACE and gene cloning

Purified RNA was used to synthesize the 3'- or 5'-RACE-ready cDNA with the SMARTer™ RACE cDNA Amplification Kit (Clontech Laboratories, Cal., USA). To acquire the full-length cDNA sequences, it was necessary to perform 3' and 5' RACE reactions, which were done following the user's manual and using gene specific primers based on the corresponding sequences from the *T. wilfordii* transcriptome sequencing dataset (Table S7). The full-length ORFs were cloned by PCR amplification using PrimeSTAR GXL DNA Polymerase (Takara Biotechnology, Dalian, China), according to the manufacturer's instructions, then ligated into the pMD19-T vector (Takara Biotechnology, Dalian, China) and verified by complete sequencing.

Sequence analysis

The sequences of the cDNA for *TwTPS7v2, TwCPS2, TwTPS3v2, TwTPS9v2, TwTPS27v2, TwKSL1*, and *TwTPS16v2* were analyzed at NCBI (http://www.ncbi.nlm.nih.gov/). The open reading frames (ORFs) and deduced amino acid sequences were determined using the online tool ORF Finder (http://www.ncbi.nlm.nih.gov/gorf/gorf.html) and the ExPASy online tool (http://web.expasy.org/translate/), respectively.

Although none of the *T. wilfordii* diterpene synthases identified here were exactly identical to those recently reported by others (Anderson-Ranberg *et al.,* 2016; Hansen *et al.,* 2017a), most were similar enough to be allelic and were named accordingly. In particular, given the 96.8%, 98.9%, 99.3%, 98.5%, and 98.0% identities (at the amino acid sequence level) to the previously characterized *ent*-CPP synthase TwTPS3, CPP synthases TwTPS7 and TwTPS9, 16α-hydroxy-*ent*-kaurane synthase TwTPS16, and miltiradiene synthase TwTPS27, the corresponding enzymes were named TwTPS3v2, TwTPS7v2, TwTPS9v2, TwTPS16v2, and TwTPS27v2, respectively. By contrast, TwKSL1 shares less than 95% identity with any of the previously characterized diterpene synthases.

For phylogenetic analysis, amino acid sequences for a variety of diterpene synthases were obtained from the NCBI database (Table S8), and a tree constructed with the MEGA6 software package (Tamura *et al.,* 2013) using the neighbor-joining method. One thousand bootstrap replicates were performed in each analysis to define the level of confidence support.

Sub-cellular localization

All constructs for *N. benthamiana* transformation were prepared using the E3025 vector (Jin 2008), which contains a gene for the green fluorescent protein (GFP) driven by the 35S

Author Manuscript Author Manuscript Author Manuscript Author Manuscript

promoter, and the specific primers were listed in Table S7. The recombinant plasmids containing the ORFs of the targeted diterpene synthase(s) were first transformed into *Agrobacterium tumefaciens* EHA105, then injected to the *N. benthamiana* leaves, with subsequent observation via confocal laser scanning microscopy. Detailed information on subcellular localization analysis is given in the supplemental METHODS.

MeJA induction and UPLC analysis

After 10 days of cultivation, the suspension cells were treated with MeJA in carrier solution (dimethyl sulfoxide) at a final concentration of 50 μM, while cells in the control group were only treated with same volume of carrier solution. Post-induction cells were harvested in liquid nitrogen after 0, 1, 4, 12, 24, 48, 72, 120 and 240 h. Three samples were prepared for each time point in each group for UPLC analysis. Additional details are provided in the supplemental METHODS.

qRT-PCR analysis

The suspension cells harvested for UPLC analysis were also used for real-time gene expression analysis, following the procedure previously described (Su *et al.,* 2017). Expression levels were evaluated using the $2^{-\Delta\Delta Ct}$ method (Livak and Schmittgen, 2001) based on *β*-actin as the reference gene, with triplicate measurements from three biological replicates.

Recombinant expression

The relevant ORFs were amplified by PCR using PrimeSTAR GXL DNA Polymerase and gene specific primers (Table S7), then ligated into pMD19-T followed by complete sequencing and sub-cloning into the N-terminal MBP fusion expression vector pMAL-c2X (NEB, USA). The ORF for *AtKS* was amplified from an *Arabidopsis thaliana* cDNA library, and sub-cloned into the pMAL-c2X vector. *S. miltiorrhiza SmCPS1* and *SmMS* ORFs were sub-cloned into the pET32a(+) vector.

The recombinant plasmids were transformed into *E. coli TransB* (DE3) for heterologous expression, using the empty pMAL-c2X vector as a negative control. Cultures (200 mL) were grown in Luria-Bertani (LB) medium (10 g/L Tryptone, 5 g/L yeast extract, 10 g/L NaCl) containing 100 mg/L ampicillin until the optical density of the culture at 600 nm reached 0.6 to 0.8, then induced with 0.4 mM isopropyl 1-thio-*β*-D-galactopyranoside (Sigma, USA) and grown at 16 °C for 8 h at 200 rpm. The cell pellets were harvested by centrifugation (3,000 g, 20 min, 4 °C) and resuspended in 5 mL of assay buffer (50 mM HEPES, pH 7.2, 7.5 mM $MgCl_2$, 100 mM KCl, 5 mM DTT, and 5% (v/v) glycerol) and lysed by a sonicator on ice. The lysates were centrifuged (12,000 g, 30 min, 4 °C) to produce soluble extracts, which were then concentrated using Amicon Ultra-15 centrifugal filter unit with Ultracel-30 membrane (Merck Millipore, Germany), according to the manufacturer's instructions.

In vitro cell-free assays

To determine the catalytic activity of the recombinant proteins, 200 μM GGPP (Sigma-Aldrich) was added to 0.2 mL of recombinant cell-free extracts, incubated for 2 h at 25 °C in

Author Manuscript Author Manuscript Author Manuscript Author Manuscript

the dark, and then extracted with hexane (3 × 0.5 mL). Residual organic solvent was removed under a stream of N_2 before adding 10 units of calf intestinal phosphatase (CIP; NEB, USA), and then incubating for 4 h at 37 °C to allow enzymatic dephosphorylation. A standard for CPP was produced by incubation of SmCPS1 with GGPP for 2 h at 25 °C, with dephosphorylation by CIP as above. The dephosphorylated compounds were extracted with hexane (3 × 0.5 mL), with the organic extracts then completely dried under N_2 and the residue dissolved in 60 μL of hexanes for GC-MS analysis (Zhang *et al.,* 2015).

Coupled assays were performed to determine the stereochemistry of CPP much as previously described (Keeling *et al.,* 2010). Briefly, assays containing each class II TwTPS and GGPP were pre-incubated for 2 h at 25 °C, at which point equivalent volumes of cell-free extracts from individually expressed diterpene synthases (AtKS, SmMS, TwTPS27v2, TwKSL1 or TwTPS16v2) were added, along with $MgCl_2$ to a final concentration of 10 mM. These reactions were then incubated overnight at room temperature before extraction with hexane (3 × 0.5 mL), and subsequent GC-MS analysis. Production of 16α-hydroxy-*ent*-kaurane was confirmed by comparison to an authentic sample isolated from gametophores of the moss *P. patens* (Hayashi *et al.,* 2006).

Yeast expression

To confirm the results of the *in vitro* cell-free assays, the ORFs of single functional class II diterpene cyclases, as well as the functional enzymatic pairings, were PCR-amplified using gene-specific primers (Table S7), then sub-cloned into the yeast epitope-tagging vector pESC-Trp (Agilent Technologies, USA) via digestion by the corresponding restriction endonucleases. The resulting plasmids were transformed into the yeast BY-T20 strain (BY4742, *ΔTrp1, Trp1::HIS3-*P_{PGK1}*-BTS1/ERG20-*T_{ADH1}*-*P_{TDH3}*-SaGGPS-*T_{TPI1}*-*P_{TEF1}*-tHMG1-*T_{CYC1}), which produces the GGPP substrate (Dai *et al.,* 2013, 2014; Shi *et al.,* 2014), and then enzymatic activity analyzed much as previously described (Su *et al.,* 2016). Briefly, organic extracts were dried and the residues dissolved in 60 μL of hexanes for GC-MS analysis as described above.

Analysis of TwKSL1 in *E. coli*

To identify the products of TwKSL1, this was transferred to pET44a, using the *BamH*I and *Xho*I restriction sites. This was used for expression in *E. coli* strain C41 OverExpress (Lucigen) also engineered to produce *ent*-CPP, using a previously described modular metabolic engineering system (Cyr *et al.,* 2007). The resulting recombinant strain was grown in 50 mL of TB media, shaken at 200 rpm, first at 37 °C to OD_{600} ~ 0.8, then shifted to 16 °C for 1 h before induction with 1 mM IPTG, following which the culture was further shaken at 16 °C for 3 d. The resulting TwKSL1 products were directly extracted with an equal volume of hexanes, which was then separated, dried under a gentle stream of N_2, and the residue resuspended in 500 μL hexanes, with 1 μL then subjected to GC-MS analysis. Compounds were identified by comparison of retention time and mass spectra to previously characterized enzymatic products (Jia and Peters, 2016).

Author Manuscript Author Manuscript Author Manuscript Author Manuscript

Yeast two-hybrid assays

To test the interactions of TwTPS27v2 and TwTPS7v2, as well as TwTPS27v2 and TwTPS9v2. TwTPS27v2 was fused with the BD domain in the pGBKT7 vector, and TwTPS7v2 and TwTPS9v2 were individually fused with the AD domain in the pGADT7 vector. Primers used for the constructs are listed in Table S7. Yeast two-hybrid assays to assess protein interactions were performed using the yeast strain *Saccharomyces cerevisiae* AH109, as previously described (Zhai *et al.,* 2015).

Engineering yeast for miltiradiene production

To examine the catalytic efficiency of TwTPS7v2 versus TwTPS9v2, these were both sub-cloned into the vector pESC-Trp, and the resulting vector used for their co-expression in the yeast BY-T20 strain. The induced yeast cells (20 mL, cultivated for 48 h in SD-Trp-His liquid induction medium supplemented with 20 g/L D-galactose) were extracted and analyzed by GC-MS as described above.

To examine the ability of fusion to improve yield of miltiradiene, TwTPS7v2 was fused with TwTPS27v2. We constructed two modules producing the fused protein TwTPS27v2-TwTPS7v2 and TwTPS7v2-TwTPS27v2 by inserting a widely used GGGS linker encoded by a “GGT GGT GGT TCT” sequence, according to the protocol of *pEASY*®-Uni Seamless Cloning and Assembly Kit (TransGen Biotech, Beijing, China). The recombinant plasmids pESC-Trp::TwTPS7v2/TwTPS27v2, pESC-Trp::TwTPS7v2-TwTPS27v2 and pESC-Trp::TwTPS27v2-TwTPS7v2 were transformed into BY-T20, induced with D-galactose. The products were then analyzed by GC-MS as described above. Linear calibration was performed to calculate the yield of miltiradiene (R^2 = 0.9997).

Site-directed mutagenesis of TwCPS2 and TwTPS16v2

Site-directed mutagenesis of the DXDD motif of TwCPS2 (DTDC^{311}TAM to DTDD^{311}TAM), and the active site of TwTPS16v2 (DLLKSA^{608}LRE to DLLKSM^{608}LRE) were performed with the relevant pMAL-c2X construct using mutagenic primers (Table S7) and the Fast Mutagenesis System (TransGen Biotech), according to the manufacturer's instructions. Expression and functional characterization of these mutants was carried out as described above.

RNAi

Vector pK7GWIWG2D (Invitrogen, USA) was used for RNAi targeting *TwTPS7v2* and *TwTPS9v2*, or *TwTPS27v2*, in suspension cells. Briefly, fragments of *TwTPS7v2/TwTPS9v2* or *TwTPS27v2* were ligated to vector pK7GWIWG2D using the Gateway cloning system (Invitrogen) and the resulting vectors transformed into suspension cells.

Suspension cells in the logarithmic growth phase were plated on MS solid medium supplemented with 0.5 mg/L 2,4-D, 0.1 mg/L KT, and 0.5 mg/L IBA, and 30 g/L sucrose (pH = 5.8), and grown for 7 days before bombardment. Then the recombinant plasmids were transformated into the cells using a biolistic gene gun (PDS 100/He, Bio-Rad). Each transformation was performed twice. The resulting recombinant cells were cultured for 7 days before UPLC analysis.

Author Manuscript Author Manuscript Author Manuscript Author Manuscript

Supplementary Material

Refer to Web version on PubMed Central for supplementary material.

Acknowledgments

We thank Prof. Xueli Zhang for providing the yeast strain BY-T20 (Tianjin Institute of Industrial Biotechnology, Chinese Academy of Sciences, China), Prof. Meng Wang for the *N. benthamiana* seeds and assistance with subcellular localization (Institute of Genetics and Developmental Biology Chinese Academy of Sciences), and Dr. Kawaide for the gift of authentic 16α-hydroxy-*ent*-kaurane isolated from gametophores of the moss *P. patens* (Tokyo University of Agriculture and Technology, Japan). This work was supported by the National Natural Science Foundation of China (81422053 and 81373906 to W.G, and 81325023 to L.H.), Key project at central government level: The ability establishment of sustainable use for valuable Chinese medicine resources (2060302) to L.H., National High Technology Research and Development Program of China (863 Program: 2015AA0200908) and Support Project of High-level Teachers in Beijing Municipal Universities in the Period of 13th Five-year Plan (CIT&TCD20170324) to W.G., as well as a grant from the US National Institutes of Health (GM109773) to R.J.P.

References

Andersen-Ranberg J, Kongstad KT, Nielsen MT, et al. Expanding the landscape of diterpene structural diversity through stereochemically controlled combinatorial biosynthesis. Angew. Chem. Int. Ed. Engl. 2016; 55:2142–2146. [PubMed: 26749264]

Chen F, Tholl D, Bohlmann J, Pichersky E. The family of terpene synthases in plants: a mid-sized family of genes for specialized metabolism that is highly diversified throughout the kingdom. Plant J. 2011; 66:212–229. [PubMed: 21443633]

Chen YW, Lin GJ, Chia WT, Lin CK, Chuang YP, Sytwu HK. Triptolide exerts anti-tumor effect on oral cancer and KB cells *in vitro* and *in vivo*. Oral. Oncol. 2009; 45:562–568. [PubMed: 19359213]

Chugh R, Sangwan V, Patil SP, et al. A preclinical evaluation of Minnelide as a therapeutic agent against pancreatic cancer. Sci. Transl. Med. 2012; 4:156ra139.

Cyr A, Wilderman PR, Determan M, Peters RJ. A modular approach for facile biosynthesis of labdane-related diterpenes. J. Am. Chem. Soc. 2007; 129:6684–6685. [PubMed: 17480080]

Dai ZB, Liu Y, Zhang X, Shi MY, Wang B, Wang D, Huang LQ, Zhang XL. Metabolic engineering of *Saccharomyces cerevisiae* for production of ginsenosides. Metab. Eng. 2013; 20:146–156. [PubMed: 24126082]

Dai ZB, Wang B, Liu Y, Shi MY, Wang D, Zhang X, Liu T, Huang LQ, Zhang XL. Producing aglycons of ginsenosides in bakers' yeast. Sci. Rep. 2014; 4:3698–3698. [PubMed: 24424342]

Del Sal G, Manfioletti G, Schneider C. The CTAB-DNA precipitation method: A common mini-scale preparation of template DNA from phagemids, phages or plasmids suitable for sequencing. Biotechniques. 1989; 7:514–520. [PubMed: 2699240]

Forman V, Callari R, Folly C, Heider H, Hamberger B. Production of Putative Diterpene Carboxylic Acid Intermediates of Triptolide in Yeast. Molecules. 2017; 22:981.

Gao JP, Sun S, Li WW, Chen YP, Cai DF. Triptolide protects against 1-methyl-4-phenyl pyridinium-induced dopaminergic neurotoxicity in rats: implication for immunosuppressive therapy in Parkinson's disease. Neurosci. Bull. 2008; 24:133–142. [PubMed: 18500385]

Gao W, Hillwig ML, Huang LQ, Cui GH, Wang XY, Kong JQ, Yang B, Peters RJ. A functional genomics approach to tanshinone biosynthesis provides stereochemical insights. Org. Lett. 2009; 11:5170–5173. [PubMed: 19905026]

Gao Y, Honzatko RB, Peters RJ. Terpenoid synthase structures, a so far incomplete view of complex catalysis. Nat. Prod. Rep. 2012; 29:1153–1175. [PubMed: 22907771]

Gong Y, Xue B, Jiao J, Jing L, Wang X. Triptolide inhibits COX-2 expression and PGE2 release by suppressing the activity of NF-kappaB and JNK in LPS-treated microglia. J. Neurochem. 2008; 107:779–788. [PubMed: 18761708]

Grabherr MG, Haas BJ, Yassour M, et al. Full-length transcriptome assembly from RNA-Seq data without a reference genome. Nat. Biotechnol. 2011; 29:644–652. [PubMed: 21572440]

Author Manuscript Author Manuscript Author Manuscript Author Manuscript

Hansen NL, Heskes AM, Hamberger B, Olsen CE, Hallström BM, Andersen-Ranberg J, Hamberger B. The terpene synthase gene family in *Tripterygium wilfordii* harbors a labdane-type diterpene synthase among the monoterpene synthase TPS-b subfamily. Plant J. 2017a; 89:429–441. [PubMed: 27801964]

Hansen NL, Nissen JN, Hamberger B. Two residues determine the product profile of the class II diterpene synthases TPS14 and TPS21 of *Tripterygium wilfordii*. Phytochemistry. 2017b; 138:52–56. [PubMed: 28279524]

Hayashi K, Kawaide H, Notomi M, Sakigi Y, Matsuo A, Nozaki H. Identification and functional analysis of bifunctional *ent*-kaurene synthase from the moss *Physcomitrella patens*. FEBS Lett. 2006; 26:6175–6181.

Inabuy F, Fischedick JT, Lange I, Hartmann M, Srividya N, Parrish AN, Xu M, Peters RJ, Lange BM. Biosynthesis of diterpenoids in *Tripterygium* adventitious root cultures. Plant Physiol. 2017; 175:92–103. [PubMed: 28751314]

Irmisch S, Müller AT, Schmidt A, Günther J, Gershenzon J, Köllner T. One amino acid makes the difference: the formation of *ent*-kaurene and 16α-hydroxy-*ent*-kaurane by diterpene synthases in poplar. BMC Plant Biol. 2015; 15:262. [PubMed: 26511849]

Jia M, Peters RJ. Extending a single residue switch for abbreviating catalysis in plant *ent*-kaurene synthases. Front. Plant Sci. 2016; 7:1765. [PubMed: 27920791]

Jin, JC. Cloning and preliminary functional study of the NAD^+-dependent sorbitol dehydrogenase (NAD-SDH) in Tobacco. master thesis. Henan Agricultural University; Henan, China: 2008.

Kawaide H, Hayashi K, Kawanabe R, Sakigi Y, Matsuo A, Natsume M, Nozaki H. Identification of the single amino acid involved in quenching the *ent*-kauranyl cation by a water molecule in *ent*-kaurene synthase of *Physcomitrella patens*. FEBS J. 2011; 278:123–133. [PubMed: 21122070]

Kitaoka N, Lu X, Yang B, Peters RJ. The application of synthetic biology to elucidation of plant mono-, sesqui-, and diterpenoid metabolism. Mol. Plant. 2015; 8:6–16. [PubMed: 25578268]

Keeling CI, Dullat HK, Yuen M, Ralph SG, Jancsik S, Bohlmann J. Identification and functional characterization of monofunctional *ent*-copalyl diphosphate and *ent*-kaurene synthases in white spruce reveal different patterns for diterpene synthase evolution for primary and secondary metabolism in gymnosperms. Plant Physiol. 2010; 152:1197–1208. [PubMed: 20044448]

Kupchan SM, Court WA, Dailey RG Jr, Gilmore CJ, Bryan RF. Triptolide and tripdiolide, novel antileukemic diterpenoid triepoxides from *Tripterygium wilfordii*. J. Am. Chem. Soc. 1972; 94:7194–7195. [PubMed: 5072337]

Kutney JP, Beale MH, Salisbury PJ, et al. Triptolide from tissue culture of *Tripterygium wilfordii*. Heterocycles. 1980; 14:1465–1467.

Kutney JP, Han K. Studies with plant-cell cultures of the Chinese herbal plant, *Tripterygium wilfordii*. Isolation and characterization of diterpenes. Recl. Trav. Chim. Pays-Bas. 1996; 115:77–93.

Leuenroth SJ, Bencivenga N, Chahboune H, Hyder F, Crews CM. Triptolide reduces cyst formation in a neonatal to adult transition Pkd1 model of ADPKD. Nephrol. Dial. Transplant. 2010; 25:2187–2194. [PubMed: 20139063]

Li FQ, Cheng XX, Liang XB, Wang XH, Xue B, He QH, Wang XM, Han JS. Neurotrophic and neuroprotective effects of tripchlorolide, an extract of Chinese herb *Tripterygium wilfordii* Hook F, on dopaminergic neurons. Exp. Neurol. 2003; 179:28–37. [PubMed: 12504865]

Li FQ, Lu XZ, Liang XB, Zhou HF, Xue B, Liu XY, Niu DB, Han JS, Wang XM. Triptolide, a Chinese herbal extract, protects dopaminergic neurons from inflammation-mediated damage through inhibition of microglial activation. J. Neuroimmunol. 2004; 148:24–31. [PubMed: 14975583]

Livak KJ, Schmittgen TD. Analysis of relative gene expression data using real-time quantitative PCR and the $2^{-\Delta\Delta Ct}$ method. Methods. 2001; 25:402–408. [PubMed: 11846609]

Manzo SG, Zhou ZL, Wang YQ, Marinello J, He JX, Li YC, Ding J, Capranico G, Miao ZH. Natural product triptolide mediates cancer cell death by triggering CDK7-dependent degradation of RNA polymerase II. Cancer Res. 2012; 72:5363–5373. [PubMed: 22926559]

Morrone D, Chambers J, Lowry L, Kim G, Anterola A, Bender K, Peters RJ. Gibberellin biosynthesis in bacteria: separate *ent*-copalyl diphosphate and *ent*-kaurene synthases in *Bradyrhizobium japonicum*. FEBS Lett. 2009; 583:475–480. [PubMed: 19121310]

Author Manuscript Author Manuscript Author Manuscript Author Manuscript

Nie J, Zhou M, Lü C, Hu X, Wan B, Yang B, Li Y. Effects of triptolide on the synaptophysin expression of hippocampal neurons in the AD cellular model. Int. Immunopharmacol. 2012; 13:175–180. [PubMed: 22498763]

Peters RJ. Two rings in them all: the labdane-related diterpenoids. Nat. Prod. Rep. 2010; 27:1521–1530. [PubMed: 20890488]

Shi MY, Liu Y, Wang D, Lu FP, Huang LQ, Dai ZB, Zhang XL. Construction of Saccharomyces cerevisiae cell factories for lycopene production. Zhongguo Zhong Yao Za Zhi. 2014; 39:3978–3985. [PubMed: 25751950]

Su P, Cheng QQ, Wang XJ, Cheng XQ, Zhang M, Tong YR, Li F, Gao W, Huang LQ. Characterization of eight terpenoids from tissue cultures of the Chinese herbal plant, *Tripterygium wilfordii*, by high-performance liquid chromatography coupled with electrospray ionization tandem mass spectrometry. Biomed. Chromatogr. 2014; 28:1183–1192. [PubMed: 25237706]

Su P, Tong YR, Cheng QQ, Hu YT, Zhang M, Yang J, Teng ZQ, Gao W, Huang LQ. Functional characterization of *ent*-copalyl diphosphate synthase, kaurene synthase and kaurene oxidase in the *Salvia miltiorrhiza* gibberellin biosynthetic pathway. Sci. Rep. 2016; 6:23057. [PubMed: 26971881]

Su P, Hu TY, Liu YJ, Tong YR, Guan HY, Zhang YF, Zhou JW, Huang LQ, Gao W. Functional characterization of NES and GES responsible for the biosynthesis of (*E*)-nerolidol and (*E,E*)-geranyllinalool in *Tripterygium wilfordii*. Sci. Rep. 2017; 7:40851. [PubMed: 28128232]

Tamura K, Stecher G, Peterson D, Filipski A, Kumar S. MEGA6: molecular evolutionary genetics analysis version 6.0. Mol. Biol. Evol. 2013; 30:2725–2729. [PubMed: 24132122]

Tao X, Lipsky PE. The Chinese anti-inflammatory and immunosuppressive herbal remedy *Tripterygium wilfordii* Hook F. Rheum. Dis. Clin. North Am. 2000; 26:29–50. [PubMed: 10680192]

Titov DV, Gilman B, He QL, Bhat S, Low WK, Dang Y, Smeaton M, Demain AL, Miller PS, Kugel JF. XPB, a subunit of TFIIH, is a target of the natural product triptolide. Nat. Chem. Biol. 2011; 7:82–188.

Tu SH. Difficulties and countermeasures in treatment of rheumatoid arthritis with *Tripterygium*. Chin J. Integr. Tradit. West Med. 2009; 29:104–105.

Yamaguchi S, Sun TP, Kawaide H, Kamiya Y. The GA2 locus of *Arabidopsis thaliana* encodes ent-kaurene synthase of gibberellin biosynthesis. Plant Physiol. 1998; 116:1271–1278. [PubMed: 9536043]

Zerbe P, Chiang A, Bohlmann J. Mutational analysis of white spruce (*Picea glauca*) *ent*-kaurene synthase (PgKS) reveals common and distinct mechanisms of conifer diterpene synthases of general and specialized metabolism. Phytochemistry. 2012; 74:30–39. [PubMed: 22177479]

Zhai QZ, Zhang X, Wu FM, Feng HL, Deng L, Xu L, Zhang M, Wang QM, Li CY. Transcriptional mechanism of jasmonate receptor COI1-mediated delay of flowering time in *Arabidopsis*. Plant Cell. 2015; 27:2814–2828. [PubMed: 26410299]

Zhang M, Su P, Zhou YJ, Wang XJ, Zhao YJ, Liu YJ, Tong YR, Hu TY, Huang LQ, Gao W. Identification of geranylgeranyl diphosphate synthase genes from *Tripterygium wilfordii*. Plant Cell Rep. 2015; 34:2179–2188. [PubMed: 26449416]

Zheng Y, Zhang WJ, Wang XM. Triptolide with potential medicinal value for diseases of the central nervous system. CNS Neurosci. Ther. 2013; 19:76–82. [PubMed: 23253124]

Zhou YJ, Gao W, Rong QX, et al. Modular pathway engineering of diterpenoid synthases and the mevalonic acid pathway for miltiradiene production. J. Am. Chem. Soc. 2012; 134:3234–3241. [PubMed: 22280121]

Zi J, Peters RJ. Characterization of CYP76AH4 clarifies phenolic diterpenoid biosynthesis in the Lamiaceae. Org. Biomol. Chem. 2013; 11:7650–7652. [PubMed: 24108414]

Zi J, Mafu S, Peters RJ. To gibberellins and beyond! Surveying the evolution of (di)terpenoid metabolism. Annu. Rev. Plant Biol. 2014; 65:259–286. [PubMed: 24471837]

Author Manuscript Author Manuscript Author Manuscript Author Manuscript

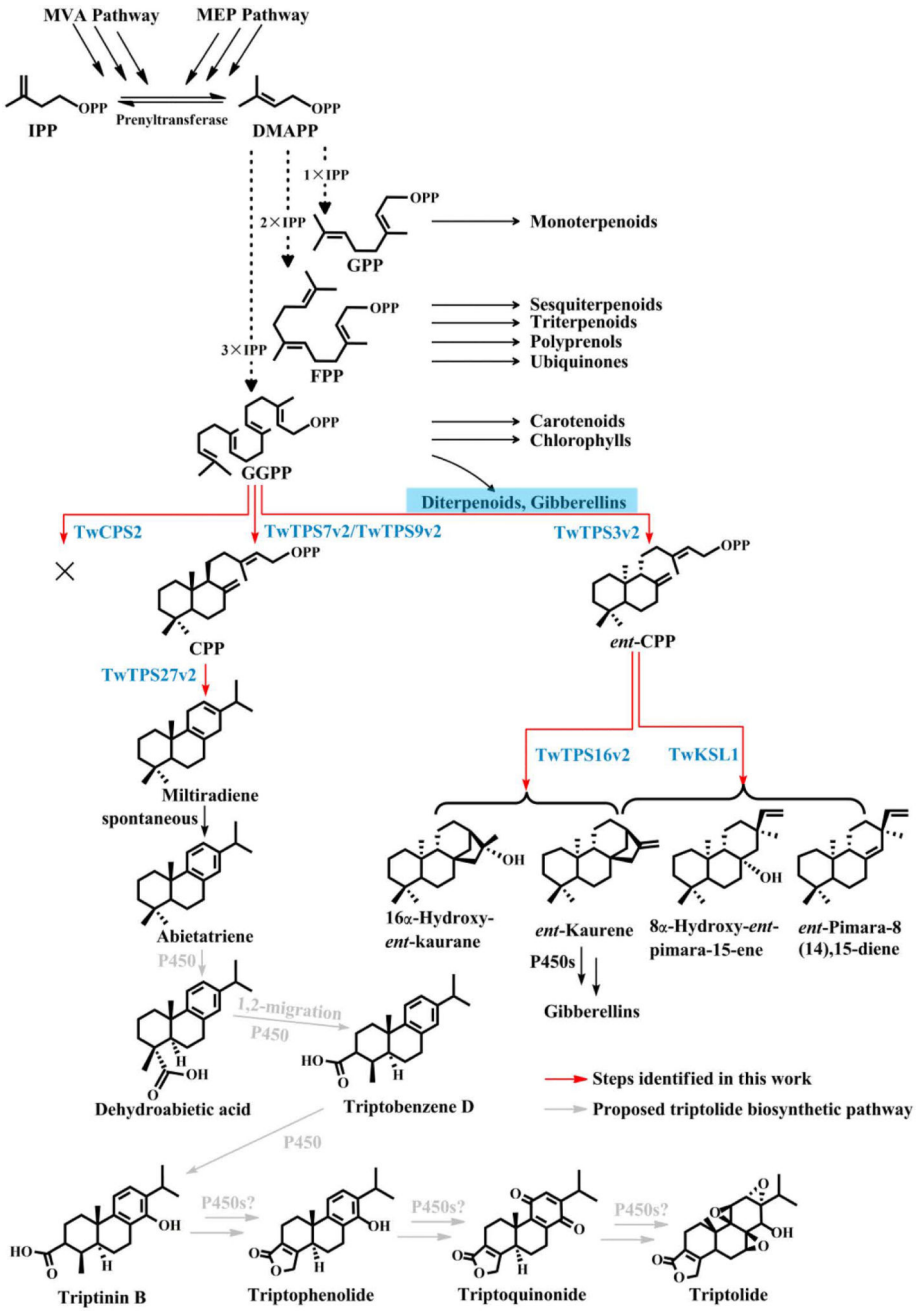

Figure 1.

Diterpenoid biosynthetic network in *T. wilfordii* as elucidated by the work described here and others (Forman *et al.,* 2017; Inabuy *et al.,* 2017).

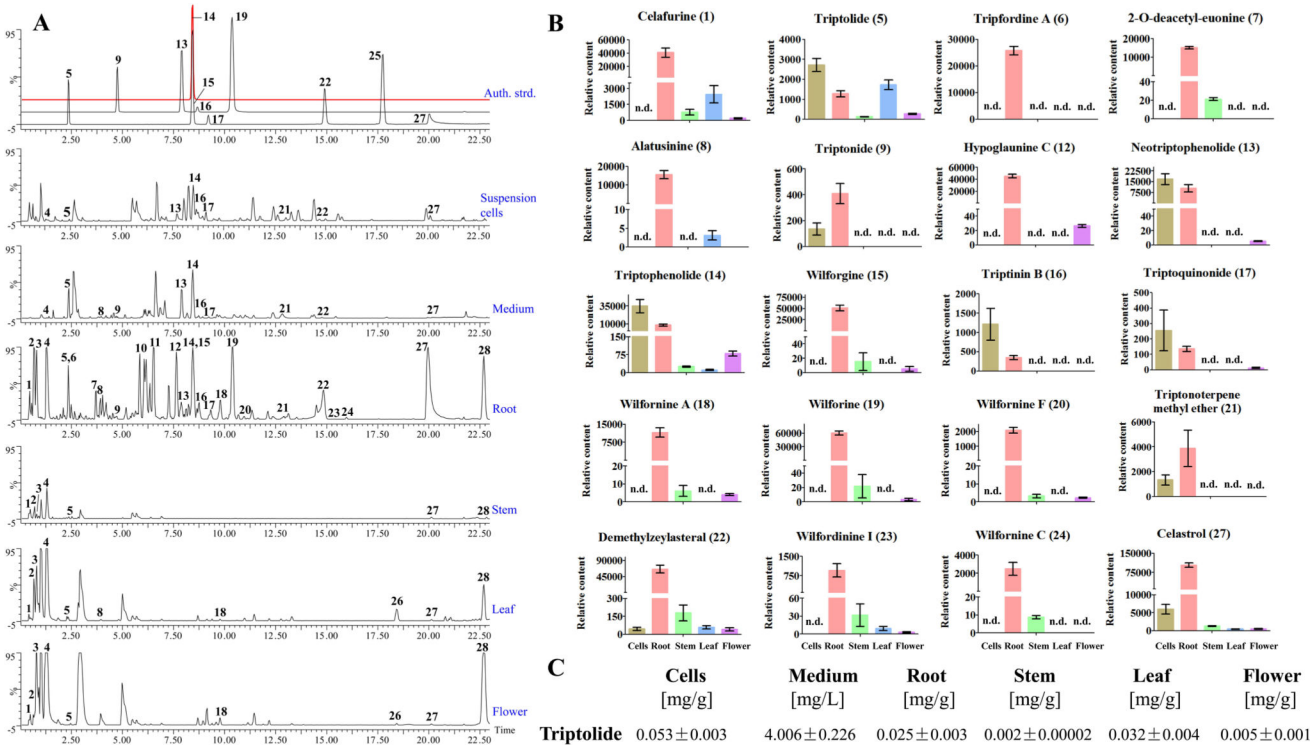

Figure 2.

Comparison of extracts from *T. wilfordii* suspension cells and whole plant organs. **(A)** BPI chromatograms of extracts from suspension culture cells and medium, and plant root, stem, leaf, and flower tissues by UPLC/Q-TOF MS. The identities of the metabolite peaks 1 to 28 are listed in Table 1. **(B)** Relative content of the identified metabolites from suspension cells, culture medium, root, stem, leaf, or flower. **(C)** Concentrations of triptolide in suspension cells, culture medium, root, stem, leaf, or flower.

Author Manuscript Author Manuscript Author Manuscript Author Manuscript

Author Manuscript Author Manuscript Author Manuscript Author Manuscript

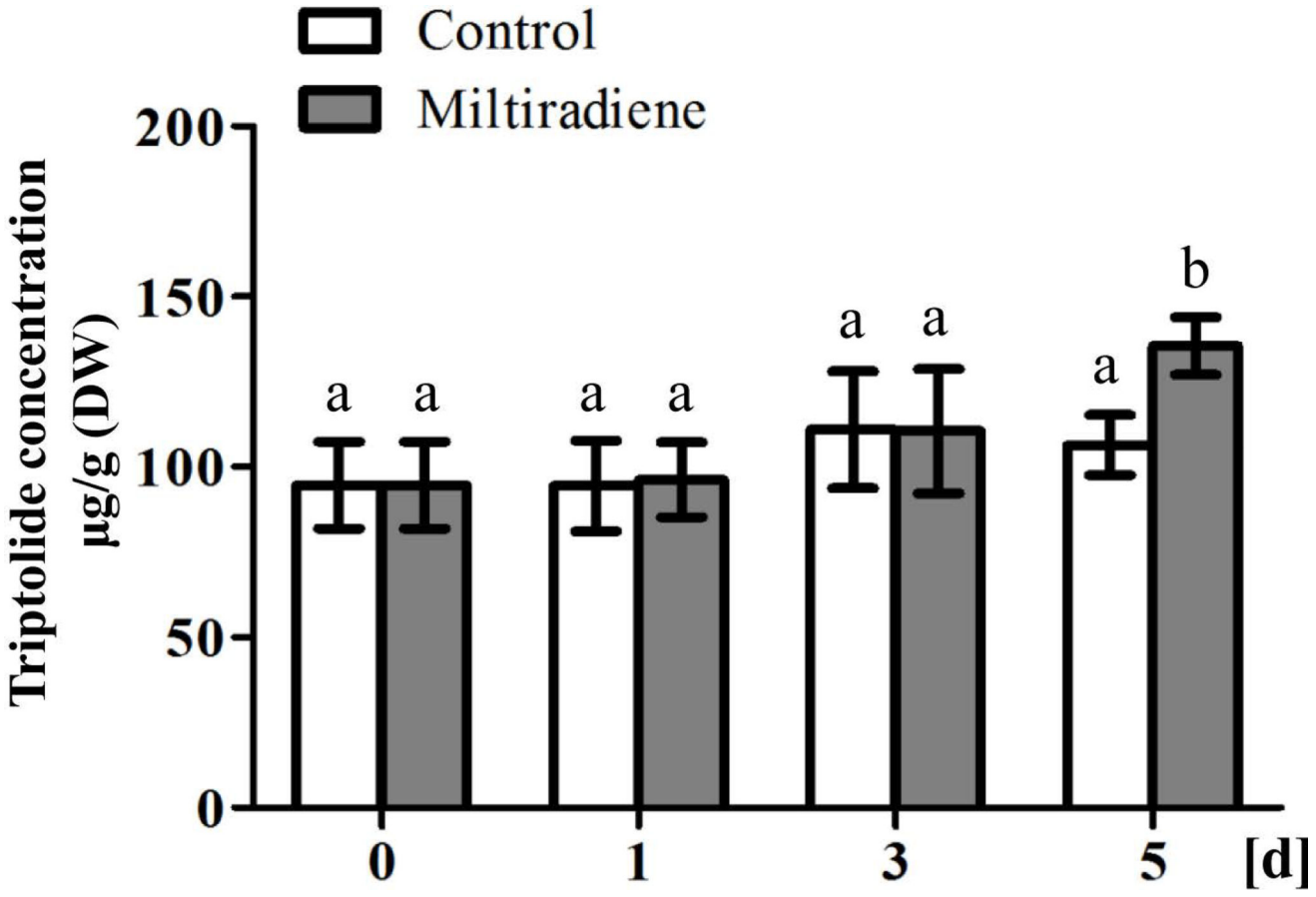

Figure 3.

Triptolide content in suspension cells fed with miltiradiene as measured by UPLC. The data represent the averages ± standard deviations from analysis of at least four independent lines of suspension cell cultures (lettering indicates statistically significant difference from all-by-all comparison using the Student's t-test).

Author Manuscript Author Manuscript Author Manuscript Author Manuscript

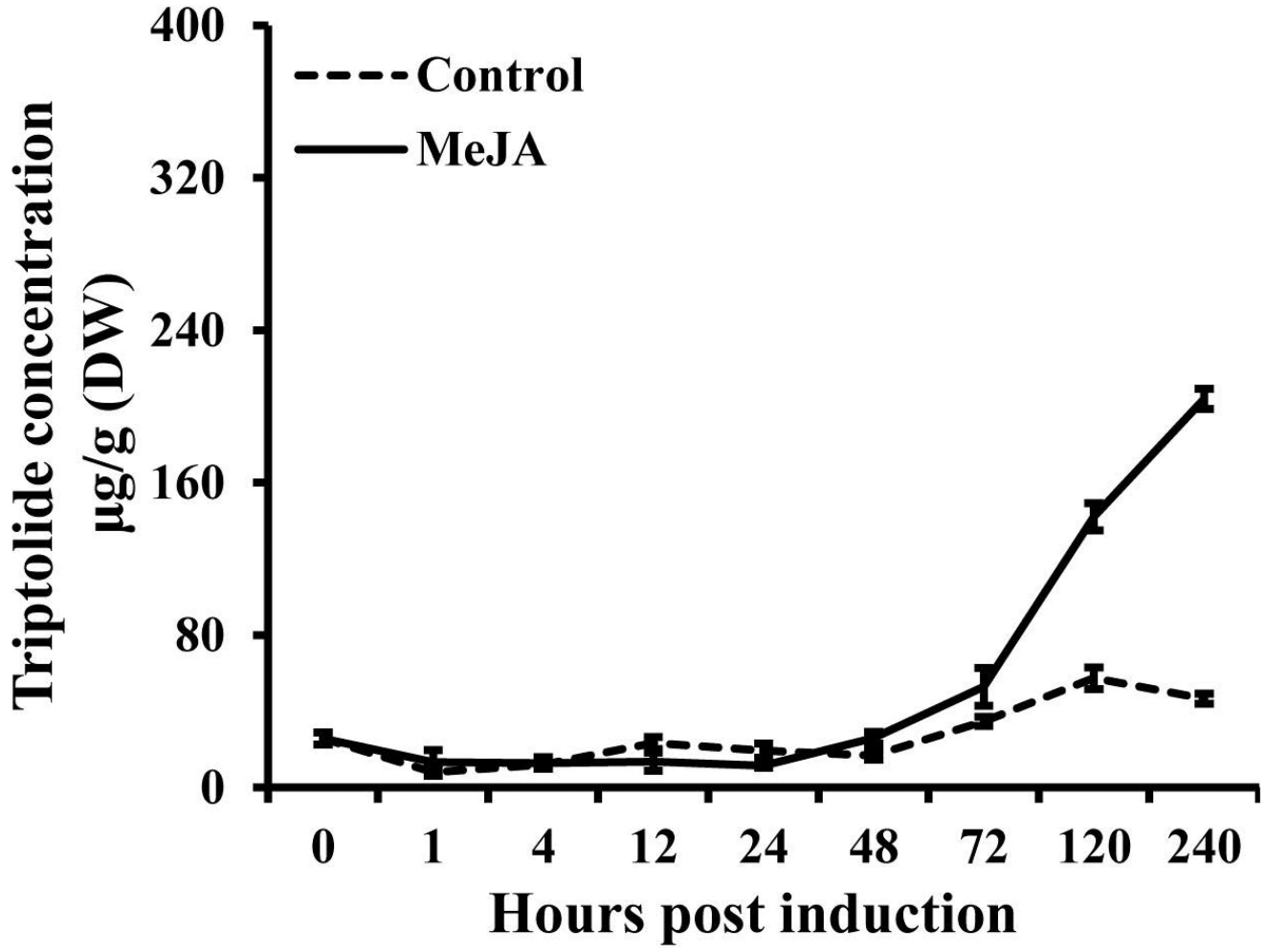

Figure 4.

Accumulation of triptolide in suspension cells induced by MeJA. The data represent the averages ± standard deviations of at least three independent suspension cell cultures.

Author Manuscript Author Manuscript Author Manuscript Author Manuscript

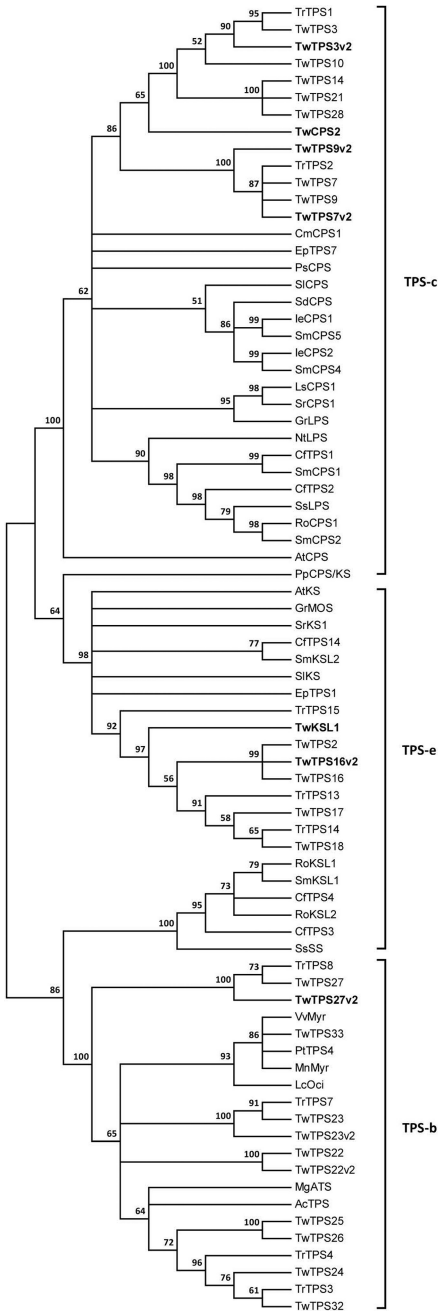

Figure 5.

Phylogenetic tree of *T. wilfordii* diterpene synthases (i.e., those from the TPS-c and TPS-e sub-families) with representative examples from other species. Abbreviations and NCBI accession numbers are provided in Table S8.

Author Manuscript Author Manuscript Author Manuscript Author Manuscript

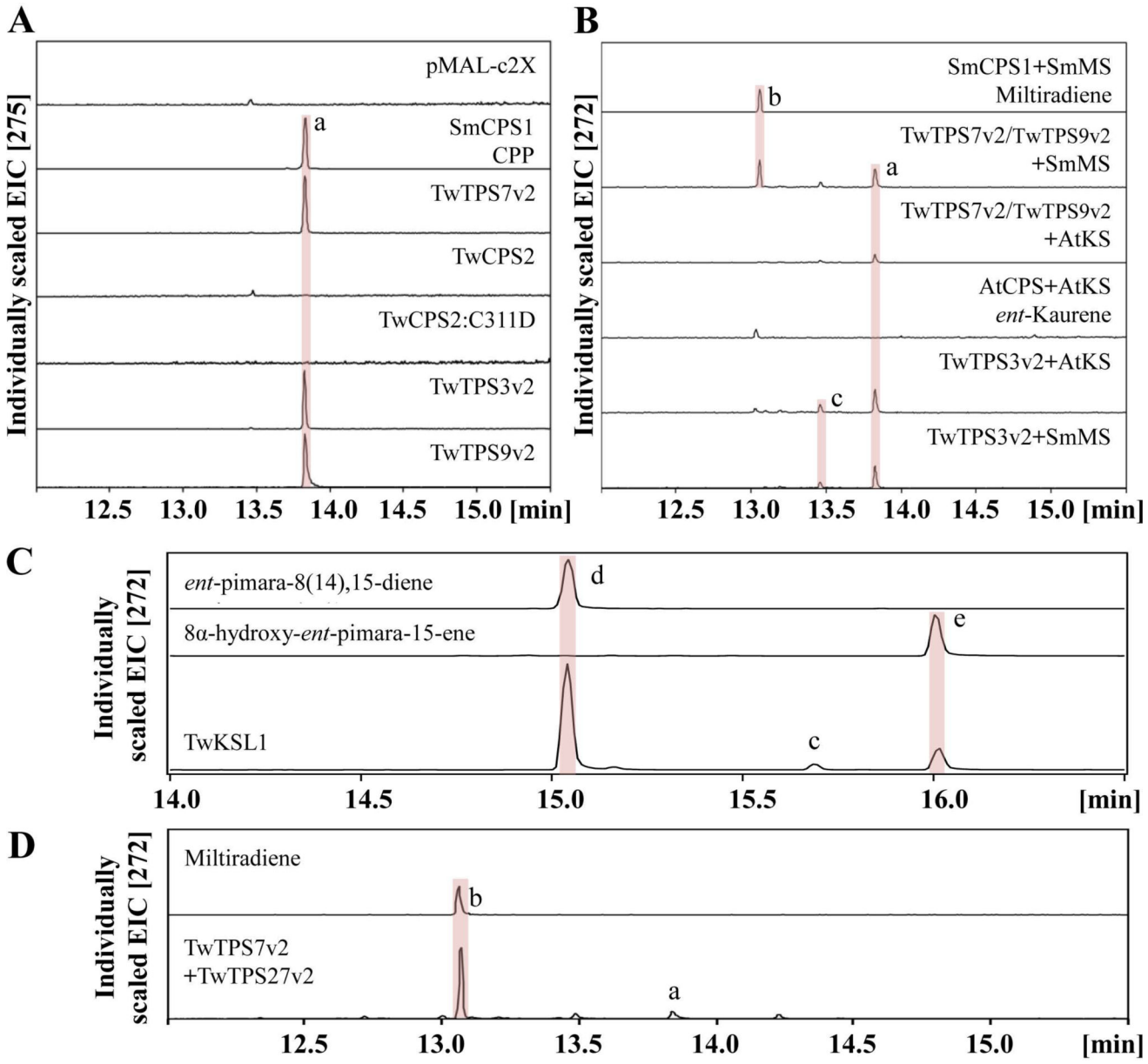

Figure 6.

GC-MS analysis of the products from the reactions catalyzed by *T. wilfordii* (di)terpene synthases *in vitro*. **(A)** GC-MS analysis of the dephosphorylated reaction products of recombinant TwCPSs with GGPP as substrate, compared with CPP produced by SmCPS1, which is detected here as the dephosphorylated copalol. **(B)** GC-MS analysis of TwTPS7v2, TwTPS3v2 or TwTPS9v2 coupled with either SmMS or AtKS, compared with the miltiradiene or *ent*-kaurene produced by the complementary enzymatic pairs SmCPS1 and SmMS or AtCPS and AtKS, respectively. **(C)** GC-MS analysis of the TwKSL1 reaction products with *ent*-CPP. **(D)** GC-MS analysis of the reaction products from TwTPS27v2 and TwTPS7v2 with GGPP. Peaks are lettered as follows: a, (*ent*-)copalol (from dephosphorylated (*ent*-)CPP); b, miltiradiene; c, *ent*-kaurene; d, *ent*-pimara-8(14),15-diene; e, 8α-hydroxy-*ent*-pimar-15-ene.

Author Manuscript Author Manuscript Author Manuscript Author Manuscript

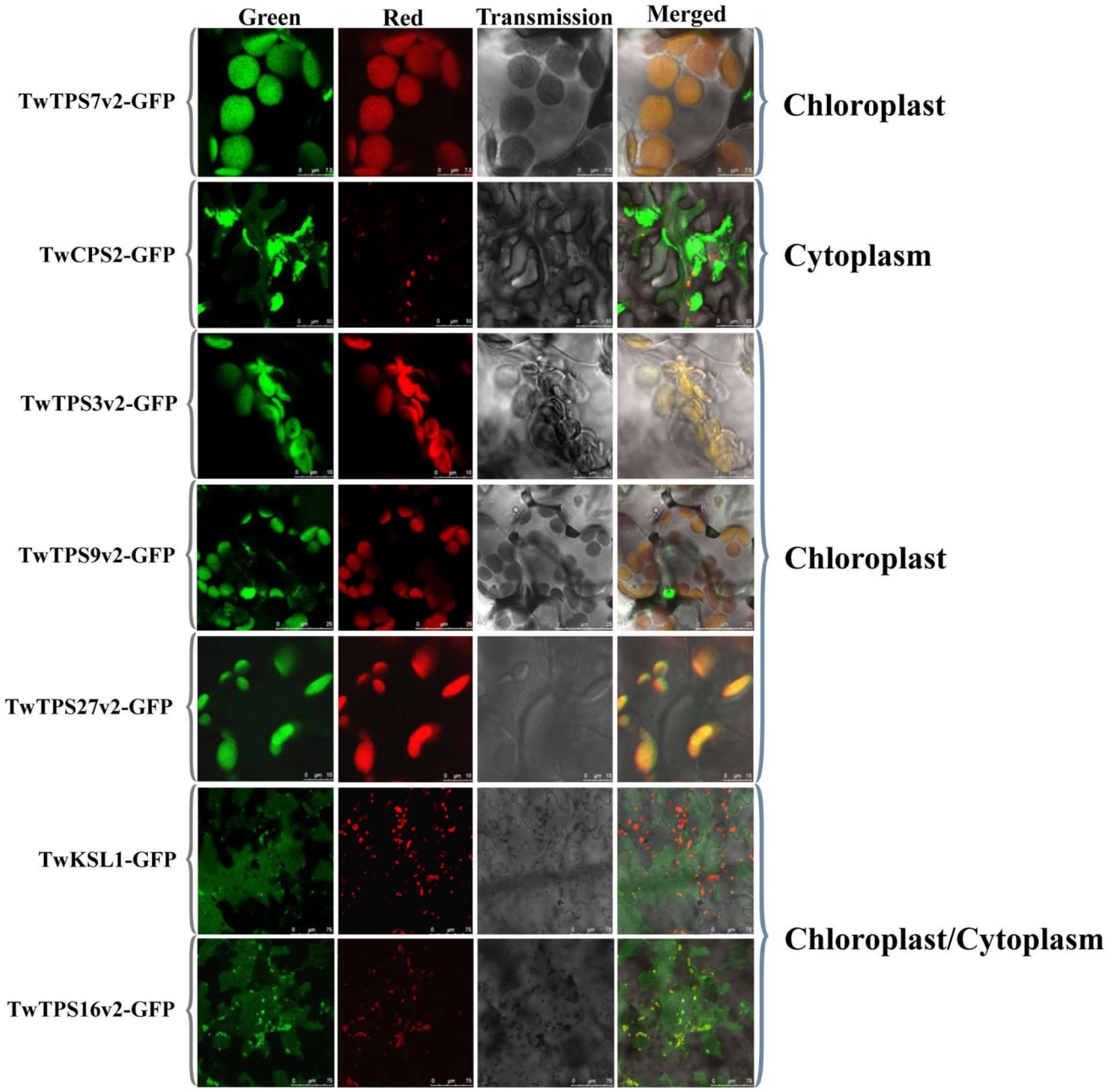

Figure 7.

Subcellular localization of *T. wilfordii* diterpene synthases with GFP fusion protein in *N. benthamiana* leaves. Images were taken with a confocal laser scanning microscope. Green, GFP fluorescence image; Red, chlorophyll autofluorescence image; Transmission, bright-field image; Merged, merger of these images. Bars, 7.5 μm (TwTPS7v2-GFP), 50 μm (TwCPS2-GFP), 10 μm (TwTPS3v2-GFP), 7.5 μm (TwTPS9v2-GFP), 10 μm (TwTPS27v2-GFP), 75 μm (TwKSL1-GFP), 75 μm (TwTPS16v2-GFP).

Author Manuscript Author Manuscript Author Manuscript Author Manuscript

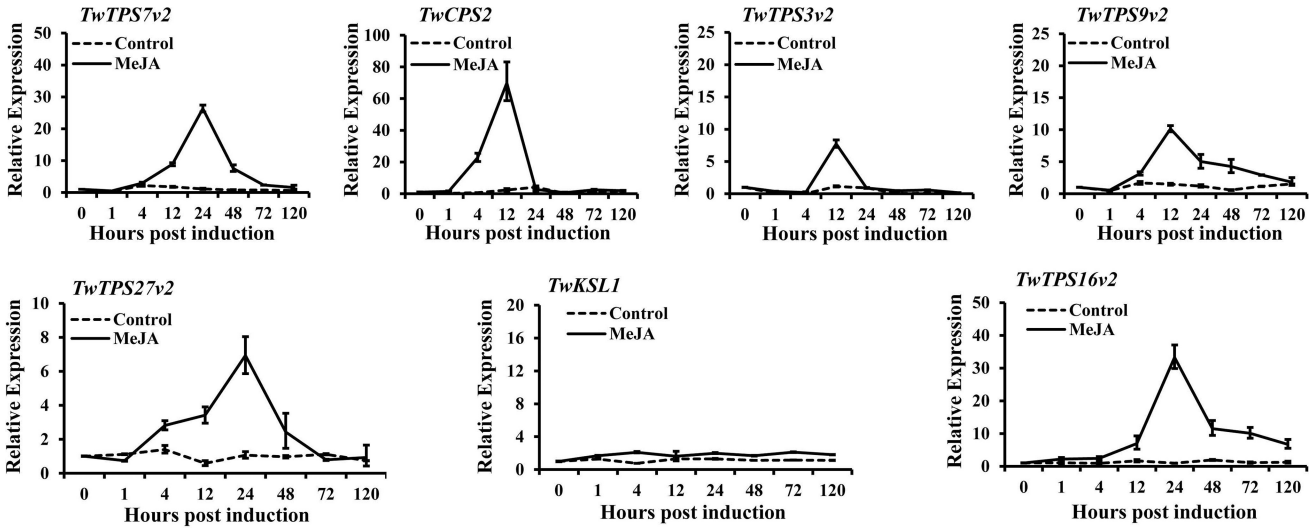

Figure 8.

Relative expression of *T. wilfordii* diterpene synthases in suspension cells treated with MeJA. MeJA, suspension cells treated with 50 μM MeJA; Control, suspension cells treated with carrier solution (dimethyl sulfoxide). The X axis represents the hours after treatment (0, 1, 4, 12, 24, 48, 72, 120, 240 h).

Author Manuscript Author Manuscript Author Manuscript Author Manuscript

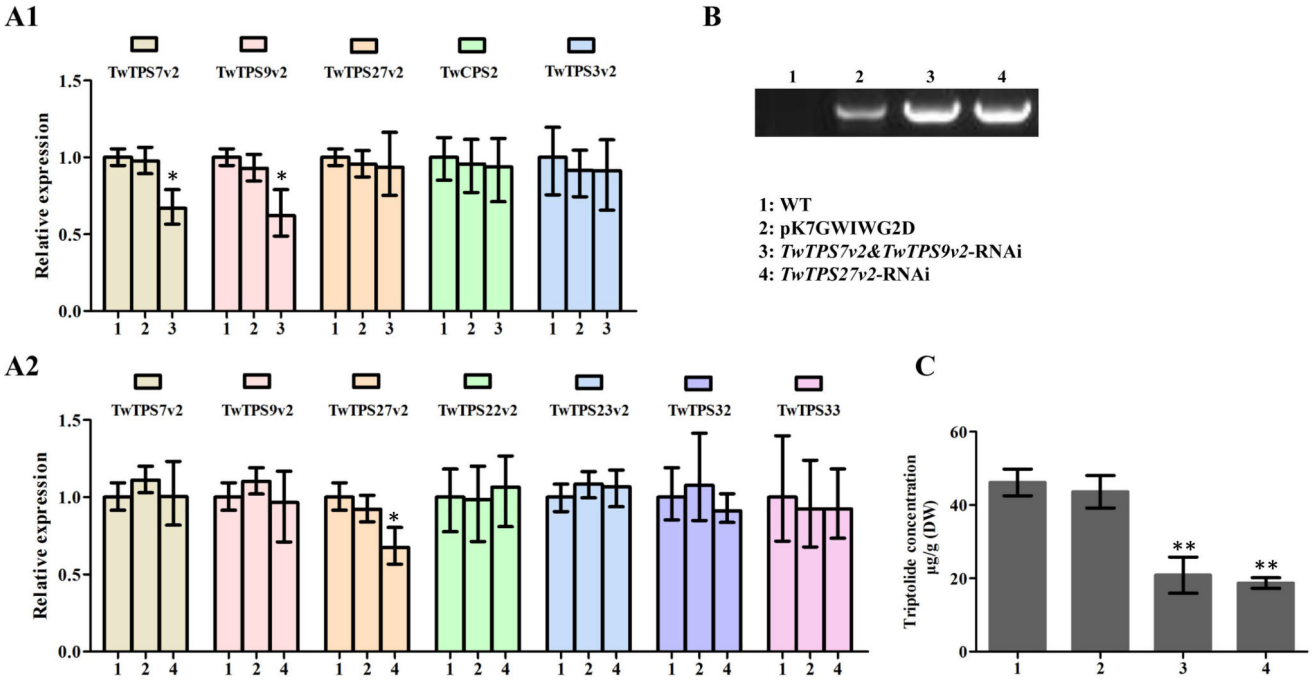

Figure 9.

Relative expression of *TwTPS7v2, TwTPS9v2, TwTPS27v2*, and closely related *TPS*s, as well as triptolide concentration in RNAi suspension cells. **(A1)** Relative expression of *TwTPS7v2, TwTPS9v2, TwTPS27v2*, as well as the related TPS-c sub-family members *TwCPS2* and *TwTPS3v2* in *TwTPS7v2&TwTPS9v2*-RNAi suspension cells. **(A2)** Relative expression of *TwTPS7v2, TwTPS9v2*, and *TwTPS27v2*, as well as related TPS-b sub-family members *TwTPS22v2, TwTPS23v2, TwTPS32* and *TwTPS33*, in *TwTPS27v2*-RNAi suspension cells. **(B)** Presence of recombinant RNAi plasmids, as detected by PCR. **(C)** Triptolide concentration in RNAi suspension cells. The data represent the averages ± standard deviations of at least four independent lines of suspension cells (* $P < 0.05$, ** $P < 0.01$).

Author Manuscript Author Manuscript Author Manuscript Author Manuscript

Plant J. Author manuscript; available in PMC 2019 January 01.

Table 1

Metabolites detected by UPLC-QTOF-MS in in all tissues (root, stem, leaf, and flower) of *T. wilfordii*, and suspension cells as well as the mediums.

Metabolite Number in Fig. 1	RT [min]	Formula	$[M+H]^+$ Calculated	$[M+H]^+$ Observed	Error [Δppm]	MS/MS signal patterns (% relative abundance)	Auth. strd. confirmed	Tentative ID
Celafurine (1)	0.53	$C_{21}H_{27}O_3N_3$	370.2131	370.2140	2.4	370(7.2), 317(18.1), 305(37.1), 287(54.1), 263(25.6), 179(26.1), 139(62.3), 127(35.9), 100(21.1)		√
Unknown alkaloid (2)	0.67	$C_{20}H_{27}O_2N_5$	370.2243	370.2270	7.3	370(11.3), 265(3.4), 249(5.8), 166(9.9), 161(16.1), 160(100), 131(5.6), 100(23.9)		
Unknown alkaloid (3)	0.81	$C_{21}H_{33}O_5N$	380.2437	380.2437	0	380(13.1), 275(2.2), 259(4.0), 188(3.5), 176(8.4), 161(14.0), 105(36.8), 100(13.5)		
Unknown alkaloid (4)	1.30	$C_{23}H_{35}O_5N$	406.2593	406.2601	2.0	406(20.9), 301(5.4), 258(6.2), 188(7.7), 161(12.3), 160(99.2), 131(100), 103(13.2)		
Triptolide (5)	2.35	$C_{20}H_{24}O_6$	361.1651	361.1656	1.4	361(100), 279(2.1), 250(2.2), 201(5.1), 157(2.9), 145(3.6), 108(6.6), 105(2.6)	√	
Tripfordine A (6)	2.35	$C_{36}H_{45}O_{18}N$	780.2715	780.2704	1.4	780(52.2), 752(100), 734(24.1), 674(11.7), 632(11.7), 204(10.4), 194(29.7), 176(23.8), 158(2.4)		√
2-O-deacetyl-euonine (7)	3.71	$C_{36}H_{45}O_{17}N$	764.2766	764.2759	0.9	764(100), 746(51.2), 686(16.8), 644(8.9), 206(72.0), 160(2.9)		√
Alatusinine (8)	3.92	$C_{38}H_{47}O_{19}N$	822.2821	822.2823	0.2	822(41.3), 794(100), 776(12.2), 674(12.0), 250(6.2), 194(17.2), 176(19.1), 160(6.5)		√
Triptonide (9)	4.73	$C_{20}H_{22}O_6$	359.1495	359.1500	1.4	359(100), 197(1.6), 171(2.1), 143(3.1), 107(3.0)	√	
Unknown alkaloid (10)	5.85	$C_{35}H_{46}O_{20}N_3$	828.2675	828.2670	0.6	828(43.1), 806(100), 788(25.9), 746(18.8), 686(20.6), 644(3.6), 206(40.6), 178(10.2)		
Unknown alkaloid (11)	6.52	$C_{35}H_{46}O_{20}N_3$	828.2675	828.2673	0.2	828(37.9), 806(100), 788(50.0), 746(48.6), 704(14.8), 686(12.0), 609(5.9), 206(21.5), 160(6.5)		
Hypoglaunine C (12)	7.67	$C_{43}H_{49}O_{19}N$	884.2977	884.2984	0.8	884(69.0), 856(100), 838(15.0), 674(12.1), 194(11.3), 176(14.4), 105(6.4)		√
Neotriptophenolide (13)	7.88	$C_{21}H_{26}O_4$	343.1909	343.1931	6.4	343(86.4), 301(17.8), 297(36.9), 257(22.3), 255(100), 240(32.6), 205(50.2), 177(18.8), 163(35.1), 137(10.7)	√	
Triptophenolide (14)	8.44	$C_{20}H_{24}O_3$	313.1804	313.1822	5.7	313(31.0), 271(9.7), 253(9.1), 225(47.8), 206(100), 178(20.4), 133(10.6), 106(16.1)	√	
Wilforgine (15)	8.44	$C_{41}H_{47}O_{19}N$	858.2821	858.2871	5.8	858(100), 840(22.3), 798(9.4), 780(4.8), 746(8.3), 686(15.4)	√	
Triptinin B (16)	8.65	$C_{20}H_{26}O_3$	315.1960	315.1969	2.9	297(33.8), 279(24.2), 269(27.8), 255(100), 237(47.8), 227(41.5), 213(34.4), 197(29.2), 185(38.6), 171(78.1), 157(34.7), 149(40.4), 147(48.0), 133(39.8), 105(12.0)	√	
Triptoquinonide (17)	9.21	$C_{20}H_{22}O_4$	327.1596	327.1611	4.6	327(100), 309(6.0), 281(77.6), 263(24.5), 253(24.1), 239(62.4), 224(17.4), 211(18.6), 193(15.0), 169(16.7), 165(12.1), 143(6.9), 119(7.9), 108(5.9)	√	
Wilfornine A (18)	9.81	$C_{45}H_{51}O_{20}N$	926.3083	926.3055	3.0	926(38.5), 804(100), 760(11.3), 744(6.1), 684(6.0), 204(6.6)		√

Author Manuscript Author Manuscript Author Manuscript Author Manuscript

Metabolite Number in Fig. 1	RT [min]	Formula	[M+H]$^+$ Calculated	Observed	Error [Δppm]	MS/MS signal patterns (% relative abundance)	Auth. strd. confirmed	Tentative ID
Wilforine (19)	10.41	$C_{43}H_{49}O_{18}N$	868.3028	868.3049	2.4	868(100), 850(33.6), 808(12.6), 746(14.6), 686(25.2), 206(30.7), 178(7.1), 105(4.8)	√	
Wilfornine F (20)	10.97	$C_{41}H_{47}O_{17}N$	826.2922	826.2901	2.5	826(74.4), 812(100), 808(38.6), 748(6.6), 310(4.7), 206(43.4), 105(5.6)		√
Triptonoterpene methyl ether (21)	12.93	$C_{21}H_{30}O_3$	331.2273	331.2281	2.4	316(17.6), 301(16.0), 271(21.3), 245(21.3), 231(19.9), 206(59.6), 201(27.4), 179(100), 163(31.5), 137(24.6), 109(9.0), 105(6.2)		√
Demethylzeylasteral (22)	14.85	$C_{29}H_{36}O_6$	481.2590	481.2603	2.7	481(100), 463(3.2), 245(6.5), 231(62.1), 213(5.0), 203(14.4), 161(1.5), 147(4.5), 121(1.8), 109(4.6)	√	
Wilfordinine I (23)	15.41	$C_{48}H_{51}O_{19}N$	946.3134	946.3094	4.2	946(41.0), 918(7.8), 846(12.7), 824(100), 764(6.8), 746(4.4), 625(2.0), 204(5.8)		√
Wilfornine C (24)	15.97	$C_{50}H_{53}O_{20}N$	988.3239	988.3201	3.8	988(34.1), 960(5.5), 942(3.9), 920(1.9), 888(1.8), 866(100), 848(6.5), 822(4.8), 806(3.8), 788(1.6), 764(3.9), 746(3.9), 204(4.7), 105(4.4)		√
Dehydroabietic acid (25)	17.76	$C_{20}H_{28}O_2$	301.2168	301.2163	1.7	173(83.1), 171(8.0), 159(16.7), 140(25.4), 133(60.1), 131(100), 106(58.6)	√	
Unknown alkaloid (26)	18.42	$C_{34}H_{35}O_9N_4$	643.2404	643.2399	0.8	643(100), 583(59.2), 555(21.5), 495(15.2), 469(3.1), 441(3.0), 118(0.9)		
Celastrol (27)	20.00	$C_{29}H_{38}O_4$	451.2848	451.2864	3.5	451(3.1), 215(15.5), 202(16.7), 201(100), 186(7.9), 153(11.3), 128(8.5), 115(7.1)	√	
Unknown alkaloid (28)	20.69	$C_{29}H_{42}O_{10}N_4$	607.2979	607.2989	1.6	607(100), 547(33.2), 461(3.7)		√

Plant J. Author manuscript; available in PMC 2019 January 01.